View metadata, citation and similar papers at core.ac.uk

brought to you by CORE

provided by European Journal of Chemistry

European Journal of Chemistry 3 (1) (2012) 57-64

European Journal of Chemistry

Journal homepage: www.eurjchem.com

Synthesis, structural elucidation and antimicrobial effectiveness of coordination entities of cobalt (II) and nickel (II) derived from 9,17-diaza-2,6,11,15-tetrathia-1,7,10,16-(1,2)-tetrabenzenacyclooctadecaphan-8,17-diene

Rajiv Kumar[a,*], Rajni Johar[b] and Anil Krishan Aggarwal[a]

[a] *Department of Chemistry, Shivaji College University of Delhi, New Delhi, 110027, India*
[b] *Department of Chemistry, Guru Govind Singh Indraprashtha University, New Delhi, 110002, India*

**Corresponding author at: Department of Chemistry, Shivaji College University of Delhi, New Delhi, 110027, India. Tel.: +91.98.10742944; fax: +91.11.25155551. E-mail address: chemistry_rajiv@hotmail.com (R. Kumar).*

ARTICLE INFORMATION

Received: 24 April 2011
Received in revised form: 01 June 2011
Accepted: 17 June 2011
Online: 31 March 2012

KEYWORDS

EPR
Antimicrobial
Molecular modeling
Potential separation
Splitting parameters
Coordination entities

ABSTRACT

9,17-Diaza-2,6,11,15-tetrathia-1,7,10,16-(1,2)-tetrabenzenacyclooctadecaphan-8,17-diene, macrocycle was synthesized, thereafter formulation and designing strategies applied for the preparation of coordination entities of Co(II) and Ni(II). Coordination behaviour of N_2S_4 donor macrocycle towards metal ion(s) was assessed by physiochemical measurements and spectral investigations *viz.* elemental analysis, molar conductance, magnetic susceptibility measurements, infrared, UV-Vis, ^1H and ^{13} C NMR, mass spectroscopy, electron paramagnetic resonance (EPR), cyclic voltammetry and molecular modeling. Side-by-side comparison of the spectral findings exposed different geometrical aspects of macrocycle and coordination entities. Cyclic voltammogram showed fully oxidized and reduced species in one unified experiment. Macrocycle and coordination entities were screened for antimicrobial effectiveness (antifungal properties against *Aspergillus-niger*).

1. Introduction

The ligand binds metal ion(s) to form mixed multi-functional materials capable of furnishing ligand field strength around metal ion(s) to develop molecular recognitions. Ligand works as a system limit adverse effects of metal ion(s) overload, inhibit selected metalloenzymes activity, facilitate metal ion(s) re-distribution, detect and detoxify toxic metals. Their synthetic protocols depend significantly on the dimensions of their internal cavity, rigidity of ligand, nature of donor atoms and as a whole the great availability as ligand with coordinating abilities of anion(s) involved [1,2].

Macrocycle (MC) and its derivatives act as donor centre capable of performing various specific molecular activities with perfect use to design and develop magnetic resonance imaging (MRI) contrasting agents, radiopharmaceuticals and chemotherapeutics [3,4]. Further, computational calculations offer a deep appreciation in theoretical interest and evaluation of practical findings to determine their great availability and flexibility as ligand.

Biotransformational enzymes and their cofactors can be explored with the help of such hypothetical calculations to design good models [5]. Herein, N_2S_4 donor coordination entities of Co(II) and Ni(II) were derived from macrocycle i.e. 9,17-diaza-2,6,11,15-tetrathia-1,7,10,16-(1,2)-tetrabenzen acyclooctadecaphan-8,17-diene. An explanatory note is presented having spectral findings on selection and coordination potential of donor atoms of macrocycle with metal(s). Molecular models for coordination entities (CEs) were obtained to get minimum energy through computational calculation. Inhibiting potential (antifungal against *Aspergillus-niger*) was screened and results obtained were arranged graphically.

2. Experimental

2.1. Materials and Chemicals

All the chemicals used were of Analytical Reagent grade procured from Sigma-Aldrich. Metal salts were purchased from E. Merck. All reagents were used without further purification.

2.2. Instrumentation

Analytical data (C, H and N) of MC and CEs were obtained with a Carlo-Ebra 1106 Elemental Analyzer. Molar conductance was measured on Leeds Northrup 4995 Conductivity Bridge. Molar magnetic susceptibility was measured with powdered samples using Faraday method. Diamagnetic corrections were made using Pascal's constant and $Hg[Co(SCN)_4]$ as calibrant at room temperature (χ_g = 16.44 ×10^{-6} in c.g.s. units). IR spectra were recorded on Perkin Elmer 137 instrument as KBr pellets in wave number region 4000-400 cm^{-1}. ^1H and ^{13}C NMR spectra were recorded at ambient temperatures on Bruker AMX400 and DRX500 spectrometers with tetramethylsilane (TMS) as internal reference and $CDCl_3$ as solvent. Chemical shifts (δ) were expressed in parts per million (ppm) relative to TMS. UV-Vis spectra were recorded on a Shimadzu UV mini 1240 spectrometer. Electron impact mass spectra were recorded on JEOL, JMS, DX-303 mass spectrometer. Electron paramagnetic resonance (EPR) spectra of CEs were recorded as polycrystalline sample as well as in solution (at room tempera-

ISSN 2153-2249 (Print) / ISSN 2153-2257 (Online) © 2012 EURJCHEM
DOI:10.5155/eurjchem.3.1.57-64.448

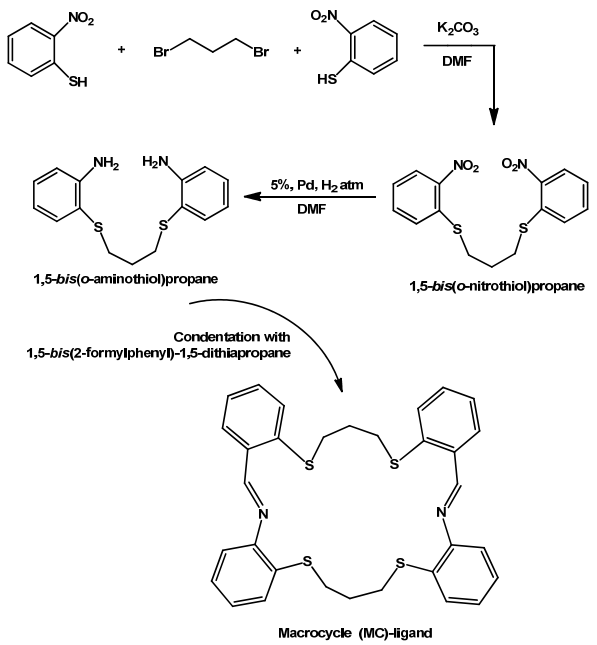

Scheme 1

-ture and liquid-nitrogen temperature (LNT)) on Varion E-4 EPR spectrometer using diphenylpicrylhydrazyl (DPPH) as the g-marker. Cyclic voltammetry measurements were made in a single compartment cell with a platinum counter electrode and Ag/Ag^+ reference electrode at room temperature. Tetraethylammonium perchlorate (TEAP) was used as a supporting electrolyte.

2.3. Synthesis

2.3.1 Synthesis of 9,17-diaza-2,6,11,15-tetrathia-1,7,10,16-(1,2)tetrabenzenacyclooctadecaphan-8,17-diene (MC)

MC having azomethine (-CH=N-) and thioether (-C_6H_4-S-CH_2-) linkages were synthesized as follows: Condensation reaction of an amine and aldehyde generated proposed macrocycle (Scheme 1). An earlier reported synthetic route [6] was followed, with slight modification, as required for the preparation of 1,5-*bis*(*o*-aminothiol)propane. A detailed methodology for the synthesis of MC with azomethine (-CH=N-) and thioether (-C_6H_4-S-CH_2-) linkages, was as follows: Hot EtOH solution (30 mL, absolute) of 1,5-*bis*(*o*-aminothiol)propane (1 mmole) was mixed with hot EtOH solution (30 mL, absolute) of 1,5-*bis*(2-formylphenyl)-1,5-dithiapropane (0.1 mol) in round bottom flask (100 mL) in presence of few drops of concentrated HCl. After complete addition, the solution mixture was refluxed for 2 h at 80-82 °C. Yellow white powdered compound was obtained, dried and dissolved in minimum amount of CH_2Cl_2. Small amount of *n*-hexane was added to precipitate out required compound and finally filtered as a dull yellow crystalline solid. The mixture was cooled at room temperature and excess solvent removed under reduced pressure until a solid product was formed. Yield: 63%. M.p.: 191 °C.

2.3.2 Synthesis of CEs

CEs of Co(II) or Ni(II) were prepared by mixing equimolar amounts of MC (0.05 mol) and corresponding metal salts, it can be $CoCl_2$ or $NiCl_2$ (0.5 mmol) in minimum quantity of EtOH (25 mL, absolute) for nearly 3-4 h at ~81-82 °C on a water bath until volume was reduced to ~12 mL.

A solid mass separated out on cooling at ~5 °C was refrigerated for better crystallization. It was then filtered, washed with EtOH and dried over P_2O_5 under vacuum. The crystals were redissolved for recrystallization with warm ethanol, resulting in a clear solution, formed small crystals when left undisturbed for weeks. CEs were soluble in DMSO, but insoluble in common organic solvents and H_2O and were thermally stable up to ~210-243 °C and then decomposed.

2.4. Molecular modeling

The MM2 option of the MacroModel 2.7 program was used with the default equations in all molecular mechanical calculations. The MacroModel force field was used to describe the organic moiety of the complex, with preference given to the MM2 parameters. Correct sequence of atoms was obtained to get reasonable low energy molecular models to determine their molecular representation in three dimensions. Complications of biochemical transformations may be explored using output obtained. An attempt to gain a better insight on the molecular structure of the ligand and its complexes, geometric optimization and conformational analysis has been performed using MM+ [7] force field.

2.5. Pharmacology (In-vitro antifungal assay)

Antimicrobial activities (antifungal) of MC and CEs were screened against *Aspergillus-niger*. Fresh stock solutions of ligand and CEs were prepared in DMSO according to required concentrations for experiments. To ensure the effect of solvent on bacterial growth, a control test was performed with test medium supplemented with DMSO.

Growth of fungus was measured by reading diameter of fungal colony. Screening for antifungal activities was carried out in vitro against *Aspergillus-niger*, following the procedure outlined [8] and their relative inhibitory ratios (%) were determined using mycelium growth rate method. On complete mycelia growth, its diameters were measured and inhibition rate was calculated according to Equation 1.

$$I = \frac{(\overline{D_I} - \overline{D_o})}{\overline{D_I}} \times 100 \quad (1)$$

where I is inhibition rate, D_I is average diameter of mycelia in the blank test and D_o being average diameter of mycelia in presence of CEs.

3. Results and discussion

3.1. Characterization of MC

3.1.1. IR spectrum of MC

No pair of bands appeared in infrared spectrum of MC at 3352-3349 and 1685 cm^{-1} corresponding to ν(-NH_2) group of 1,5-*bis*(*o*-aminothiol)propane and ν(>C=O) group of 1,5-*bis*(2-formylphenyl)-1,5-dithiapropane confirmed condensation. New medium to strong stretching vibration at 1611 cm^{-1} assigned to ν(-CH=N-)(m) appeared [9]. The characteristic ν(-CH_2-) modes of aliphatic groups were observed in the wave region 2951-2920 and 2891 cm^{-1}. A group of strong to medium intense bands were found in different wave regions 3051-3050, 1572-1550, 1165-1140 and 771-760 cm^{-1}, due to ν(Ar-CH-) aromatic stretching vibrations. Another strong to medium stretching frequency bands were observed at 810-801 cm^{-1} corresponding to ν(C-S) characteristic stretching modes [10]. FT-IR spectrum of MC have all typical features as given above were clearly compatible with the structural model of MC.

3.1.2. ^{1}H NMR spectrum of MC

^{1}H NMR spectrum of MC do not give any signal corresponding to primary amine (-NH_2) at 6.7 ppm and carbonyl (-HC=O) protons at 9.1 ppm confirmed complete condensation. Earlier evidences obtained from infrared spectrum have also suggested cyclic nature of ligand. In addition, methylene chains (-CH_2-) were detected as a bridge between two sulphur atoms at 2.70-2.60 ppm. Other multiplets were observed at 8.40-7.33 ppm (m, *J* = 8 Hz) confirming the presence of -C_6H_4-.

Another important signals were observed at 9.60-9.50 and 2.96-2.90 ppm due to the presence of azomethine (-HC=N-) and sulphur (-CH_2-S-) protons, respectively. The occurrence of this resonance in each of the above species as a 'clean' singlet confirms the presence of intact (non hydrolyzed) imine groups in each case [11]. MC is soluble in common organic solvent such as EtOH (40 °C). ^{1}H NMR (200 MHz, $CDCl_3$, δ, ppm): 9.60-9.50 (s, 2H, -CH=N-), 8.40-7.33 (m, 16H, *J* = 9.2 Hz, -C_6H_4-), 2.70-2.60 (m, 4H, *J* = 4.2 Hz, -CH_2-), 2.96-2.90 (t, 8H, J_1 = 7.8 Hz, J_2 = 8.5 Hz, -S-CH_2-).

3.1.3. ^{13}C NMR spectrum of MC

^{13}C NMR spectrum of MC displayed strong signals at δ 163.10-161.02 ppm and δ 124.60-121.10 ppm due to the presence of -CH=N- and aromatic carbon. Further, important signals were found at δ 34.20-34.00 ppm attributed to -CH_2- [12]. ^{13}C NMR (125 MHz, $CDCl_3$, δ, ppm): 124.60-121.10 (C: 2, 3, 4, 5, 8, 9, 10, 11, 12, 18, 19, 20, 21, 22, 25, 26, 27, 28), 131.01-129.64 (C: 1, 13, 17, 29), 129.23-128.02 (C: 14, 16, 30, 32), 163.10-161.02 (C: 7, 23), 151.01-150.92 (C: 6, 24), 34.20-34.00 (C: 15, 31).

3.1.4. Electron impact (EI) mass spectrum of MC

In the mass spectrum, different intensities were observed corresponding to various fragments of MC directly reflecting with their stabilities. The base peak (100%) M^+ indicated facile loss of hydrogen radical, a molecular ion peak MS (EI, *m/z* (%)): 569 (M^+) corresponds to molecular weight of MC. A general fragmentation pattern evidenced primary cleavages at hetero-carbon bonds. Beside this several other peaks of different intensities were observed having corresponding *m/z* values according to the molecular masses of different constituents [13]. Initiation in the cleavage in form of different pathways took place through the loss of fragment (-S-CH_2-CH_2-) from the parent molecule, followed by -S-CH_2- elimination as evident in mass spectrum obtained. In conclusion, presented molecular model for MC in Figure 1, is in best accordance with the elemental analysis, IR, ^{1}H NMR, ^{13}C NMR and mass spectra.

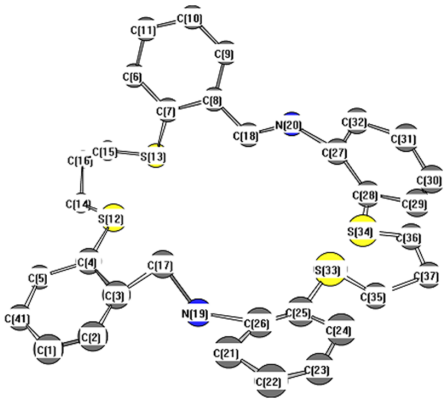

Figure 1. Molecular structure of macrocycle; Color code: C, light grey; N, blue; S, yellow.

3.2. Characterization of CEs

CEs are colored, non-hygroscopic solids, stable in air. Their chemical compositions confirmed purity and stoichiometry of neat and encapsulated CEs. Oligo and polymerization occurred after elimination of water or other molecules, finally effect the accuracy of C, H and N (Analytical data). Further results obtained had a good agreement with MS spectral findings and suggests monomeric nature of CEs. On the basis of elemental analysis arranged in Table 1, a general composition $M(L)X_2$, [where M = Co(II) and Ni(II), L = Ligand and X = Cl^-, NO_3^-, NCS^- and ½ SO_4^{2-}] was proposed. Molar conductance measurements found 170-182 $\Omega^{-1}cm^2mol^{-1}$ corresponds to 1:2 electrolytes. On the basis of results obtained, CEs were formulated as $[M(L)]X_2$.

Cavity of MC had two different donor subunits (-CH_2-S-CH_2- and -CH=N-) approached central metal ion(s) with different electron density. Qualitative reactions revealed the absence of anion(s) in $[M(L)](X)_2$ as counter ion(s).

Beside analytical analysis and spectral presentation (mass, electronic, infrared, ^{1}H and ^{13}C NMR), magnetic properties were also summarized and presented in results and discussion.

3.2.1. IR spectra of CEs

Appearance of medium to strong stretching vibrations of azomethine comparatively in lower regions at 1509-1501 cm^{-1} than the expected value 1611 cm^{-1} of MC worked as a new coordination centre. Lowering in shift in IR spectra of CEs may be explained on basis of drift of lone pair density of azomethine nitrogen towards the central metal hence confirmed encapsulation [14].

Presence of new medium strong stretching vibrations at 552-543 cm^{-1} confirmed the formation of new bonds i.e. ν(M-N) between central metal ion and nitrogen of azomethine. In addition, medium to high intense bands were observed in far infrared regions at 396-371 cm^{-1} because of bathochromic shift coupled with lower vibrational modes of S and favored it coordination with central metal [15,16]. This phenomenon attributes host/guest stability in a defined way. Related infrared spectral data were presented in Table 2.

Table 1. Molar conductance and elemental analysis of MC and CEs with Co(II) and Ni(II).

MC and CES	Molecular Formula	$\Lambda_M(\Omega^{-1}cm^2\ mol^{-1})$	Calcd. (Found) %			
			M	C	H	N
(MC-L)	$C_{32}H_{30}N_2S_4$	-	-	67.33(67.01)	5.30(5.22)	4.91(4.60)
$[Co(L)]Cl_2$	$CoC_{32}H_{30}N_2S_4Cl_2$	175	8.41(8.34)	54.85(54.65)	4.32(4.22)	4.00(3.92)
$[Co(L)](NCS)_2$	$CoC_{34}H_{30}N_4S_6$	180	7.90(7.82)	54.75(54.51)	4.05(4.01)	7.51(7.30)
$[Co(L)](NO_3)_2$	$CoC_{32}H_{30}N_4O_6S_4$	170	7.82(7.65)	50.99(50.75)	4.01(3.91)	7.43(7.40)
$[Co(L)](OSO_3)$	$CoC_{32}H_{30}N_2O_4S_5$	181	8.12(8.05)	52.95(52.65)	4.17(4.05)	3.86(3.76)
$[Ni(L)]Cl_2$	$NiC_{32}H_{30}N_2S_4Cl_2$	178	8.38(8.32)	54.87(54.67)	4.30(4.25)	4.00(3.70)
$[Ni(L)](NCS)_2$	$NiC_{34}H_{30}N_4S_6$	171	7.87(7.62)	54.76(54.62)	4.05(4.00)	7.51(7.41)
$[Ni(L)](NO_3)_2$	$NiC_{32}H_{30}N_4O_6S_4$	173	7.79(7.69)	51.00(50.63)	4.01(4.00)	7.43(7.32)
$[Ni(L)](OSO_3)$	$NiC_{32}H_{30}N_2O_4S_5$	182	8.09(8.00)	52.97(52.63)	4.17(4.11)	3.86(3.76)

Table 2. Infrared spectral data (cm^{-1}) of MC and CEs of Co(II) and Ni(II).

MC and CEs	υ(CH=N)	υ(C–H)	υ(M-N)	υ(M-S)	$\upsilon(NO_3^-)$	$\upsilon(NCS^-)$	$\upsilon(1/2\ SO_4^=)$
$C_{30}H_{26}N_2S_4(L)$	1611s	2991w	-	-	-	-	-
$[Co(L)]Cl_2$	1602s	2970w	542m	380m	-	-	-
$[Co(L)](NCS)_2$	1609s	2972w	546m	385m	-	2048s	-
$[Co(L)](NO_3)_2$	1606s	2977w	542m	341m	1385s, 824(w), 275(w)	-	-
$[Co(L)](OSO_3)$	1609s	2978w	552m	342m	-	-	1132s, 1104s, 615m
$[Ni(L)]Cl_2$	1603s	2977w	523m	390m	-	-	-
$[Ni(L)](NCS)_2$	1602s	2975w	543m	396m	-	2049s	-
$[Ni(L)](NO_3)_2$	1608s	2974w	526m	389m	1384s	-	-
$[Ni(L)](OSO_3)$	1601s	2972w	551m	387m	-	-	1131s, 1102m, 613m

3.2.2. Magnetic moments of CEs

Magnetic moments of CEs of Co(II) and Ni(II) obtained at room temperature and were usually similar to spin-only value, i.e. $\mu_{iso} = 2[S(S+1)]½$. In general, this is directly proportional to the number of unpaired electrons in metal ion(s). CEs of Ni(II) and Co(II) showed magnetic moment 2.94-2.97 and 4.76-4.91 B.M corresponding to two and three unpaired electrons, respectively. It is thus in good agreement with high spin configuration [17].

For the octahedral Co(II) (S = 3/2) complexes, the orbital angular momentum present in the ground T-term reflects heavily on the magnetic properties. On exposing complexes to D_{4h} symmetry, further splitting occurs. $^4T_{1g}$ term splits into ^4E_g and $^4A_{2g}$, where $^4A_{2g}$ is the ground state. The spin-orbit coupling splits this term into Kramers doublets Γ_6 and Γ_7. The difference of these states can be assigned as ^2D [18].

3.2.3. Electronic spectra of CEs

In the both series of CEs, *d-d* transitions were happened due to the presence of -CH=N- linkage and charge transfer transitions. Such transitions arose because of delocalization of π-electrons between central metal and donor atoms (N/S). Finally, it is a metal-to-ligand (MLCT) or ligand-to-metal (LMCT) charge (electron) transfer [19].

Electronic spectra of CEs of Co(II), three d-d transitions bands observed around 14,780-11,754 cm^{-1} and 21,624-16,710 cm^{-1}, 27,430-24,462 cm^{-1} may be assigned to $^4T_{1g}(^4F) \rightarrow {}^4T_{2g}(^4F)$ (υ_1), $^4T_{1g}(^4F) \rightarrow {}^4A_{2g}(^4F)$ (υ_2) and $^4T_{1g}(^4F) \rightarrow {}^4T_{1g}(^4P)$ (υ_3) transitions, respectively [20], characteristic of an octahedral geometry. In electronic spectra of CEs of Ni(II), three *d-d* transition bands observed around 9,920-8,410 cm^{-1}, 15,840-13,880 cm^{-1}, and 27,880-27,481 cm^{-1} may be assigned to $^1A_{1g} \rightarrow {}^1A_{2g}$, $^1A_{1g} \rightarrow {}^1B_{1g}$ (υ_1), $^1A_{1g} \rightarrow {}^1E_g$, $^3A_{1g} \rightarrow {}^3T_{2g}(F)$ (υ_2) and $^3A_{2g} \rightarrow {}^3T_{1g}(F)$ $^3A_{2g} \rightarrow {}^3T_{1g}(P)$ (υ_3) transitions, respectively, characteristic of an octahedral geometry.

3.2.4. Ligand field parameters of CEs

On basis of bands shapes and their different positions (assigned on the basis of O_h symmetry), ligand field splitting energy (Dq) and ligand field stabilization energy (LFSE) were calculated. McClure's parameters δt_{2g} and δe_g depend upon the splitting of t_{2g} and e_g orbitals observed from crystal field parameters (Ds, Dt). It confirmed π-bonding effect to be relatively more important along axial direction than σ-bonding.

σ-Bonding along with *xy*-plane was strongly related to negative sign of σ-parameter values. δ values indicate π-bonding effect to be relatively more important along the axial direction than σ-bonding. Racah inter-electronic repulsion parameter (B^l) was calculated for CEs of Co(II) using Equation 2.

$$B^l = 1/510[7(\nu_3 - 2\nu_2) + 3\{81\nu_3^2 - 16\ \nu_2(\nu_2 - \nu_3)\}^{1/2} \quad (2)$$

Values of ligand field parameters (Dq, *B*, *β* and LFSE) and lowering in *B* value from free ion value for Co(II) i.e. 1120 cm^{-1}, were determined. These results suggested 37 to 44 % covalent nature in bonding.

Racah inter-electronic repulsion parameter (B^l) was calculated by Equation 3.

$$B^l = \upsilon_2 + \upsilon_3 - 3\upsilon_1/15 \quad (3)$$

for Ni(II) complex, 10Dq = υ_1 and covalence factor (β) was obtained in the following manner, $\beta = B^l/B$, (where B is free ion value). LFSE was calculated and found equivalent to 12Dq. Due to splitting of υ_1, in electronic spectra of CEs of Ni(II), different ligand field parameters i.e. Hamiltonian parameters Ds, Dt, Dq^{xy} and Dq^z were derived from the transition energy. These values helped to figure out different geometrical features. Dq^{xy} and Dq^z were the splitting parameters directly related to the splitting in-plane and axial positions [21].

B values showed 74-75% ionic character for free ion (B° = 1041 cm^{-1}). The nephelauxetic parameters calculated had values in the range 0.81-0.78. On the basis of these values, studied MC can be fitted in the middle of the nephelauxetic series. Results obtained were helped to propose octahedral geometrical arrangement of atoms around Ni(II) and Co(II) in CEs having N_2S_4 chromophore.

3.2.5. Electron paramagnetic resonance of CEs

EPR spectra of CEs of Co(II) were recorded using DPPH as a reference standard at liquid nitrogen temperature (LNT) since the rapid relaxation of Co(II) broadened the lines at higher temperature.

CEs of Co(II) exhibited a set of six line pattern and showed a clear picture about change in configuration of electrons along their distribution around central metal atom after π-electrons interaction with MC represented in Figure 2. Values of $g_{||}$, g_{iso} and $g_\perp$ were found in range 3.95-3.70, 2.57-2.40 and 1.89-1.64, respectively. Large deviation in g values was due to large angular momentum contribution from the spin only value i.e.

2.0023. The main observed signals were typical of high-spin Co(II) complexes (S = 3/2) in a rhombically distorted octahedral complex, interpreted using an effective S = 1/2 spin Hamiltonian.

EPR spectra of CEs of Co(II), a frozen glass at 77 K showed expected ^{59}Co (I = 7/2) octet with g_{av} = 2.11 and hyperfine coupling constant A_{iso} = 38.47 G. The frozen-solution spectra indicated a rhombic system where all three axes were equivalent, consistent with the geometry of the molecule [22].

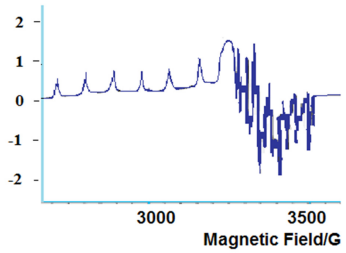

Figure 2. EPR spectrum of reduced CE of Co(II)Cl_2 at 77 K; frequency 9.47 GHz.

3.2.6. Electrochemistry of CEs

The cyclic voltammograms (CVs) of CEs were observed at oxidation and reduction potentials versus different scan rates. It was evident that used macrocycle had Lewis basicities due to the presence of N_2S_4 donor set in macrocycle (MC). The inherent kinetic stability imparted by N_2S_4 macrocycle was manifested in the electro-chemical processes of $[M(L)]X_2$ (M = Co, Ni) to generate reversible or quasi reversible redox couples in solutions.

CEs of Ni(II) showed two successive one electron processes. First one being a irreversible couple Ni(II)/Ni(I) observed at -1.48 to -1.50 (V) and assigned as Ni(II)L + e^- → Ni(I)L. The cathodic peak potential difference increased with scan rate. The peak current ratio I_{pa}/I_{pc} was found less than unity showing electron transfer reaction to follow a chemical reaction (EC mechanism).

It seemed possible that +1 oxidation state of nickel acquired d^9 or (t^6_{2g}, e^3_g) ground state electronic configuration and experiences dynamic Jahn-Teller distortion. It hence got stabilized because of possible gain in crystal field stabilization energy (CFSE).

Second electrode being an irreversible process couple each electrode couple, showed Ni(II)/Ni(III) at 1.05 to 0.97 (V) assigned as Ni(II)L → Ni(III)L + e^- peak to peak potential separation (ΔE). The approximately unit value of the cathodic to anodic peak current ratio (I_{pa}/I_{pc}) was detected for this couple within the range 0.010-1.000 Vs^{-1} scan rates. It further indicated the absence of subsequent chemical reactions and stability of the electrochemically generated Ni(III) species [23]. Figures 3 and 4 explain above discussed explanatory note.

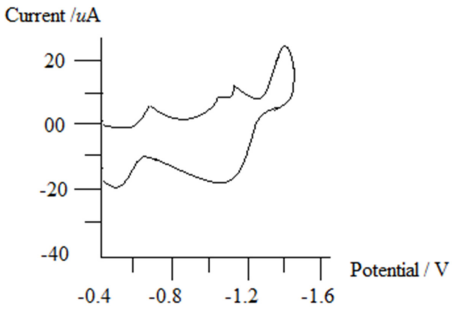

Figure 3. Cyclic voltammogram CE of Ni(II)Cl_2 in the cathodic region.

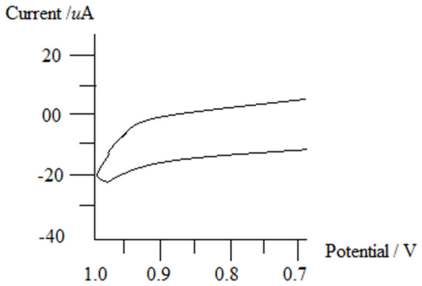

Figure 4. Cyclic voltammogram CE of Ni(II)Cl_2 in the anodic region.

Cyclic voltammograms (CVs) of CEs of Co(II) were observed in potential range 1.05 to -1.50 (V) versus Ag/AgCl for scan rate of 0.025 to 0.50 Vs^{-1}. The half-wave potentials for the reversible Co(III)/Co(II) and Co(II)/Co(I) redox couples were determined as average of cathodic and anodic peak potentials of the processes. In anodic region, one quasi-reversible oxidation process at 0.25 to 0.20 (V) was observed. In addition, it exhibited a cathodic wave at -1.25 to -1.20 (V) corresponding to Co(II) centered reduction process.

First reduction process had about a unit ratio of anodic to cathodic peak currents (I_{pa}/I_{pc}). The ratio observed for second reduction process was different and showed deviations from unity due to residual current at a low potential. The I_{pa}/I_{pc} values at slow scan rates were slightly lower than unity but increased with increasing scan rates. It was a characteristic response of a slow chemical reaction succeeding the electron transfer reaction.

These results were assigned to simple one-electron processes:

$$[Co(III)L] + e^- \rightarrow [Co(II)L]^- \quad (4)$$

and

$$[Co(II)L]^- + e^- \rightarrow [Co(I)L]^{2-} \quad (5)$$

with different values of anodic and cathodic peak separation. In controlled potential electrolysis, it was revealed that a single electron was involved in each reduction step. The low peak separation was observed for the Co(III)/Co(II) and Co(II)/Co(I) couples which explained stable behaviour of CEs and remained unchanged during the reduction processes. Electron transfer processes were not followed by a chemical reaction upon a reversal scan. $E_{0.5}$ values were found independent of scan rate but showed small dependence peak potential.

ΔE_p depends totally on scan rate observed in range 60-800 mVs^{-1}. After scanning the second cycle, no change in potential was observed in cathodic and anodic waves for these electrode processes comparatively to the reductions occurred at the same potentials as observed in the first cycle. The shifts and reversibility were apparently close to high degree of electron delocalization in CEs with N_2S_4 donor set and additional benzene units. The lower oxidation states, Co(I) was probably stabilized by thiol Schiff-base ligand unit due to sulphur atom having dπ orbitals. Imines groups played an effective role with back donation and formed equality bridges.

On increasing the number of aromatic rings or double bonds in MCs, reduction of Co(II) to Co(I) facilitates. The electro-generated Co(I) species exhibited reversible and stable character. It will likely facilitate a catalytic reduction of halogenated organic species as well as Co(III)/Co(II) species. So the oxidation processes and the splitting of the wave were based on MCs and probably due to the presence of four thiolate groups of CEs, oxidized at the different potentials.

The magnitude of half wave potential ($E_{0.5}$) generally shifts towards negative potential when metal ion chelated with

strong σ-donor ligands. The present N_2S_4 donor macrocycle, a mimic to cyclic hexadentate, behaves as a good σ-chelator through amine/thioether group. However, the position of redox wave depends on various factors such as nature of exo-cyclic substituents donor sites their π-bonding character within ligand [24].

3.2.7. Electron impact mass spectra of CEs

Mass spectral study was applied to investigate complete fragmentation patterns of Ni and Co-CEs. In electron impact mass spectra, peaks of different intensities corresponding to various fragments of CEs of Co(II) and Ni(II) were obtained along with their stabilities. A base peak M^+, indicated the facile loss of hydrogen radical at MS (EI, *m/z* (%)): 699 (M^+, 65%) and 698 (61%) a.m.u. for CEs of Co(II) and Ni(II), respectively confirmed monomeric nature of CEs and proposed formula derived from elemental analysis. General fragmentation pattern revealed primary cleavages to occur at hetero-carbon bonds. Several other peaks were observed having various *m/z* values at different intensities corresponding to molecular masses of different constituents. Their intensities gave an idea about their stabilities along with geometrical configurations [25]. The major cleavage pathways took place through the loss of -S-CH_2-CH_2- fragment, followed by the elimination of -CH_2-. In conclusion, presented generic models had 1:1 stoichiometry.

3.2.8. Molecular modeling of MC and CEs

Molecular modeling is a mathematical concept to impersonate correlated significant features i.e. molecular geometries, bond energies, torsion angles and Cartesian coordinates of concerned molecular topologies. Bond lengths, bond angles and atomic coordinates depend on the hybridization of an atom and mode of bonding. Thus, molecular modeling had been successfully used to demonstrate three dimensional arrangements of the atoms. Molecular models were proposed as a standard to judge specific interactions in topologies of the molecules of MC and derived CEs. Beside this, if deviations in distances, angles or torsion were evidenced, specific electronic interactions should perhaps be pursued.

In order to ascertain the structural features and related preferences to confirm the obtained spectral evidences. The coordination capabilities of MC towards metal ion(s) along with its impact on bond lengths and bond angles, thereby, were demonstrated and presented through the molecular models of MC and CEs. Physical dimensions of the molecules helped out to demonstrate the changes occurred during their topological assemblies. The process of determining energy minimization was repeated several times to find global minimum energy [26]. Data analysis of bond lengths and angles were presented in Table 3 to 6.

On the basis reported data, following remarks were concluded as follows:

Bond angles between metal and donor atoms in MC moiety were altered somewhat upon coordination; bonds angles S(28)-Co(39)-S(10) and S(27)-Co(39)-S(09) were 179.4° and 180.0°, respectively as a consequence of bonding. Bond angles in CEs were quite near to an octahedral geometry. It is clear that all the active groups taking part in coordination and had longer bonds than already existing in ligand in -C-S-C- and >C=N- linkages. Coordination significantly shortens as 1.8 Å for N(38)-Ni(39) as compared to 2.1 Å for S(27)-Co(39). This is because of bond lengths in MC between donor atoms probably gets affected due to the presence of hydrogen in azomethine (-CH=N-). There is a large variation in N(37)-N(38) bond lengths on complexation and becomes slightly longer as the coordination took place *via* N atom of -CH=N-.

Based on spectral and analytical analysis (elemental analysis, conductance measurements, magnetic susceptibilities, infrared, ^1H and ^{13}C NMR, electronic, mass, EPR, cyclic voltammetry and molecular modeling) solvent accessible surface model of MC and molecular models of CEs of Ni(II) were designed and presented as Figure 5 and 6.

Table 3. Selected bond lengths of CEs of Co(II).

Selected bond	Bond length, Å
S(27)-Co(39)	2.18
S(28)-Co(39)	2.18
N(37)-Co(39)	1.83
N(38)-Co(39)	1.83
S(09)-Co(39)	2.18
S(10)-Co(39)	2.18

Table 4 Selected bond lengths [Å] of CEs of Ni(II).

Selected bond	Bond length, Å
S(27)-Ni(39)	2.17
S(28)-Ni(39)	2.17
N(37)-Ni(39)	1.82
N(38)-Ni(39)	1.82
S(09)-Ni(39)	2.17
S(10)-Ni(39)	2.17

Table 5. Selected bond angles of CEs of Co(II)

Selected bond	Bond angles, °
S(28)-Co(39)-S(10)	179.4
S(27)-Co(39)-S(09)	180.0
Co(39)-N(38)-C(29)	122.1
Co(39)-N(37)-C(25)	111.0
Co(39)-N(37)-C(20)	117.3
Co(39)-S(28)-C(36)	109.5
Co(39)-S(28)-C(30)	104.0
Co(39)-S(27)-C(35)	109.5
Co(39)-S(27)-C(24)	104.0
Co(39)-S(09)-C(06)	109.5

Table 6. Selected bond angles of CEs of Ni(II).

Selected bond	Bond angles, °
N(38)-Ni(39)-S(27)	170.0
N(37)-Ni(39)-S(27)	170.0
S(28)-Ni(39)-S(27)	165.8
Ni(39)-N(38)-C(29)	111.0
Ni(39)-N(38)-C(19)	119.9
Ni(39)-N(37)-C(25)	111.0
Ni(39)-S(28)-C(36)	109.5
Ni(39)-S(28)-C(30)	104.0
Ni(39)-S(27)-C(35)	109.5
Ni(39)-S(27)-C(24)	104.0

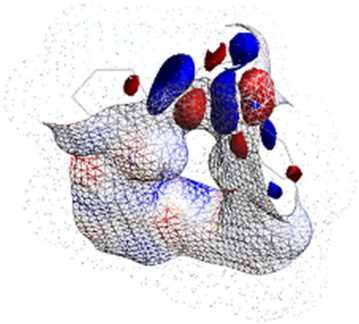

Figure 5. Solvent accessible surface model of macrocycle.

3.2.9. Pharmaceutical activities of CEs

Designing and tailoring of new biologically active CEs are crucial and depends on the utilization of new methodologies and implemented techniques significantly. Antimicrobial effectiveness of CEs depends upon several factors i.e. metal ion(s), chromophore set of MC moiety and other geometrical features. The combined impact of these factors makes MC moiety competent as desired. MCs having tailored architectures and antimicrobial effectiveness are well known. Designed CEs having appropriate metal/ligand stability within the cavity of macrocycle moiety were discussed. Moreover, coordination reduces the polarity of metal ion(s) because of partial sharing of its positive charge with donor atoms within the cavity of MC.

During this process, lipophilic nature of central metal atom increases as a result favors permeation more efficiently through the lipid layer of the microorganism to destroy them more aggressively.

Besides this, probably there may be other factors such as solubility, dipole moment and conductivity which may be influenced by metal ion(s). These could be major reasons behind the higher antimicrobial effectiveness of the CEs than MCs [27].

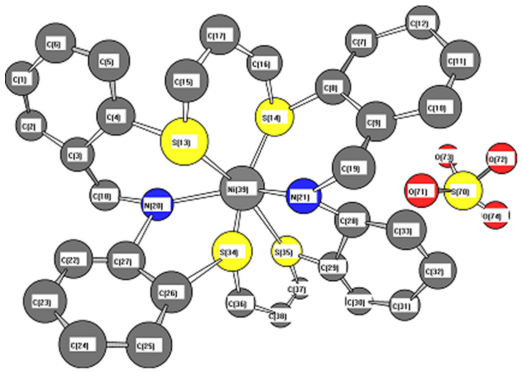

Figure 6. Molecular model of CE of Ni(II)SO_4. Color code: Ni, dark black; C, light grey; N, blue; S, yellow.

CEs were directly mixed in a medium of different concentrations. The fungus was positioned in the medium with help of an inoculum's needle. Petri dishes wrapped in polythene sheets containing some drops of C_2H_5OH were put in an incubator at 30±3 °C for 70-90 hrs. The enlargement of fungal colony was measured in diameter. Antifungal activity of MC and CEs were performed by agar plate technique against *Aspergillus-niger* and screened values were arranged graphically in Figure 7.

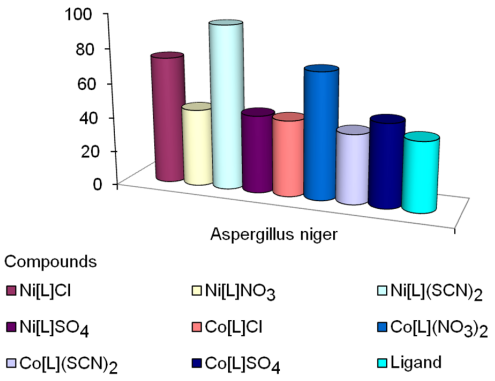

Figure 7. Comparative aspects of antifungal findings.

Results indicate that CEs have potential to generate novel antimicrobial agent by displaying moderate to high affinities for most of the receptors particularly in case of Ni(II)MC$(SCN)_2$.

Cell permeability is due to its surrounding by lipid membrane and acts as a special passage for lipid soluble materials. So, it showed liposolubility and increased antimicrobial resistance in a cell. This is known as the most important biological phenomenon in regard to antifungal aspects. Keeping in view the problem of antimicrobial resistance, reported CEs show good antimicrobial character. Polarity is directly influenced by coordination abilities of the metal because of partial sharing of its positive charge within MC system having π-electron delocalization. CEs have higher activity than free ligand because of increased activity of metal chelates according to Overtone's concept. The inhibition activity of compounds seems to govern with certain degree as per the availability percentile of sulphur atoms in MC and CEs. This is because tetrathia macrocycle shows more activity against *Aspergillus niger* compared to those having lesser number of sulphur atoms within the system.

4. Conclusions

Various properties of macrocycles i.e. dimension of internal cavity, rigidity, nature and number of donor atoms and type of anion(s) involved in coordination depend on synthetic protocols and nature of CEs significantly. Keeping in view the importance of Pederson's findings, it is a challenge to design macrocycle topologies having desired properties [28,29]. A 22-membered N_2S_4 chromophore containing MC was designed and synthesized successfully for architecture and tailoring of CEs of Ni(II) and Co(II). Molecular models confirmed the location of metal ion(s) surrounded by four sulphur and two nitrogen donor sites in equatorial plane acting as Lewis base within the cavity. The interest in such species stems from the application of these complexes ranging from modeling the active sites of many metalloenzymes to host and carry small molecules or catalysis.

CEs were screened against a fungus caused a disease black mold on certain fruits and vegetables such as grapes, onions, peanuts, as it is a common contaminant of food. CEs disturbed respiration process of cell and blocked proteins synthesis. It evidenced that hydrophobicity and steric effects comprise two major factors that govern antimicrobial effectiveness.

Electron delocalization along with main chain of -S-$(CH_2)_3$-S- bounds metal ion(s) and can be considered as a main substituent group along macrocyclic backbone or vice versa. In both situations it is important to modulate chemical and physical features of ligand and also on the properties of CEs. In electronic spectra main bands may be attributed to thio S(σ) → Co(II) (dπ) and thio S(π) → Co(II) (dπ) as ligand to metal charge transfer transitions (LMCT).

Acknowledgements

One of the authors (Rajiv Kumar) gratefully acknowledges his younger brother Bitto and sister Renu for motivation. Authors acknowledge Central Science Library, University Delhi, Delhi for providing computer facilities, Indian Institute of Technology Bombay and Indian Institute of Technology Delhi for recording EPR, ^1H NMR and ^{13}C NMR spectra respectively and to Indian Institute of Technology Roorkee, India for recording magnetic moments.

References

[1]. Saeeda, S.; Rashid, N.; Ali, M.; Hussain, R.; Jones, P. *Eur. J. Chem.* **2010**, *1(3)*, 221-227.
[2]. Aghatabay, M. N.; Mahmiani, Y.; Cevik, H.; Dulger, B. *Eur. J. Med. Chem.* **2009**, *44*, 365-372.
[3]. Aghatabay, M. N.; Bas, A.; Kircali, A.; Sen, G.; Yazicioglu, M. B.; Gucin, F.; Dulger, B. *Eur. J. Med. Chem.* **2009**, *44*, 4681-4689.
[4]. Boeyens, J. C. A.; Dobson, S. M.; Bernal, I. Stereochemical and Stereo-physical Behaviour of Macrocycles, Vol. 2. Elsevier, Amsterdam, 1987.
[5]. Lippard, S. J.; Berg, M. J. Principles of Bioinorganic Chemistry, University Science Books, Mill Valley, 1994.
[6]. Chandra, S.; Kumar, R. *Trans. Metal Chem.* **2004**, *29*, 269-275.
[7]. Allinger, N. L. *J. Am. Chem. Soc.* **1977**, *99*, 8127-8134.
[8]. Saeeda, S.; Rashida, N.; Alib, M.; Hussain, R. *Eur. J. Chem.* **2010**, *1(3)*, 200-205.
[9]. Odhiambo, R.; Muthakia, G. K.; Kagwanja, S. M. *Bull. Chem. Soc. Ethiop.* **2010**, *24(1)*, 47-58.
[10]. Mehmet, K.; Ismail, Y.; Semra, K.; Atıf, K. *Polyhedron* **2002**, *21*, 825-834.
[11]. Yuan, J. L.; Zhang, Q. L.; Liang, X.; Zhu, B. X.; Lindoy, L. F.; Wet, G. *Polyhedron* **2008**, *27*, 344-348.
[12]. Anvarhuaein, A. I.; Mohammed, I.; Wazer, M. *J. Coord. Chem.* **2005**, *58*, 529-537.
[13]. Ilhan, S.; Temel, H.; Yilmaz, I.; Sekerci, M. *J. Organomet. Chem.* **2007**, *692*, 3855-3865.

[14]. Nakamoto, K. Infrared and Raman Spectra of Inorganic and Coordination Compounds, 3rd edition, Wiley Interscience, New York, 1978.
[15]. Karadeniz, H.; Gok, Y.; Kantekin, H. *Dyes Pigm.* **2007**, *75,* 498-504.
[16]. Aghatabay, N. M.; Somer, M.; Senel, M.; Dulger, B.; Gucin, F. *Eur. J. Med. Chem.* **2007**, *42,* 1069-1075.
[17]. Kahn, O. Molecular Magnetism, VCH, New York, 1993.
[18]. Earnshaw, A. Introduction to Magnetochemistry, Academic Press, London, 1968.
[19]. Boca, R. *Struct. Bond.* **2006***, 117*, 1-264.
[20]. Lever, B. P. Electronic Spectra of the Ions in Inorganic Electronic Spectroscopy, 2nd edition, Elsevier, Amsterdam, Netherlands, 1984.
[21]. Balhausen, C. J. An Introduction to Ligand Field, McGraw Hill, New York, 1962.
[22]. Aurkie, R.; Georgina, M. R.; Ramakant, K.; Samiran, M. *Polyhedron* **2009**, *28,* 796-806.
[23]. Salih, I.; Hamdi, T.; Ismail, Y.; Memet, S. *Polyhedron* **2007**, *26,* 2795-2802.
[24]. Koca, A.; Dincer, H. A.; Kocak, M. B.; Gul, A. *Russ. J. Electrochem.* **2006**, *42(1)*, 31-37.
[25]. Meryem, N.; Yarasir, M. K.; Atıf, K.; Bekir, S. *Polyhedron* **2007**, *26*, 1139-1147.
[26]. Athanassis, C. T.; Paraskevas A. K. *Polyhedron* **2008**, *27*, 289-298.
[27]. William, H.; Stephen, V. Theory and Application of Microbiological Assays; Academic Press: San Diego, 1998.
[28]. Pedersen, C. J. Synthetic Multidentate Macrocyclic Compounds, Academic Press, New York, 1978.
[29]. Pedersen, C. J. *J. Am. Chem. Soc.* **1967**, *89*, 2495-2496.